Available online at www.sciencedirect.com
ScienceDirect
Journal of Volcanology and Geothermal Research xx (2006) xxx–xxx
Journal of volcanology and geothermal research
www.elsevier.com/locate/jvolgeores

Analysis of sustained long-period activity at Etna Volcano, Italy

Gilberto Saccorotti [a,*], Ivan Lokmer [b], Christopher J. Bean [b], Giuseppe Di Grazia [c], Domenico Patanè [c]

[a] Istituto Nazionale di Geofisica e Vulcanologia Sez. di Napoli, Osservatorio Vesuviano. Via Diocleziano, 328- 80124 Napoli, Italy
[b] School of Geological Sciences, University College Dublin. Belfield, Dublin 4, Ireland, United Kingdom
[c] Istituto Nazionale di Geofisica e Vulcanologia, Sez. di Catania. Piazza Roma, 2- 95123 Catania, Italy

Received 18 March 2006; received in revised form 9 October 2006; accepted 27 October 2006

Abstract

Following the installation of a broadband network on Mt. Etna, sustained Long- Period (LP) activity was recorded accompanying a period of total quiescence and the subsequent onset of the 2004–2005 effusive episode. From *c.* about 56000 events detected by an automatic classification procedure, we analyse a subset of about 3000 signals spanning the December 17th, 2003–September 25th, 2004, time interval. LP spectra are characterised by several, unevenly-spaced narrow peaks spanning the 0.5–10 Hz frequency band. These peaks are common to all the recording sites of the network, and different from those associated with tremor signals. Throughout the analysed time interval, LP spectra and waveforms maintain significant similarity, thus indicating the involvement of a non-destructive source process that we interpret in terms of the resonance of a fluid-filled buried cavity. Polarisation analysis indicates radiation from a non-isotropic source involving large amounts of shear. Concurrently with LP signals, recordings from the summit station also depict Very-Long-Period (VLP) pulses whose rectilinear motion points to a region located beneath the summit craters at depths ranging between 800 and 1100 m beneath the surface. Based on a refined repicking of similar waveforms, we obtain robust locations for a selected subset of the most energetic LP events from probabilistic inversion of travel-times calculated for a 3D heterogenous structure. LP sources cluster in a narrow volume located beneath the summit craters, and extending to a maximum depth of ≈800 m beneath the surface. No causal relationships are observed between LP, VLP and tremor activities and the onset of the 2004–2005 lava effusions, thus indicating that magmatic overpressure played a limited role in triggering this eruption. These data represent the very first observation of LP and VLP activity at Etna during non-eruptive periods, and open the way to the quantitative modelling of the geometry and dynamics of the shallow plumbing system.

Keywords: long-period seismicity; etna volcano; volcano monitoring; precursor

1. Introduction

Long-Period (LP) and Very-Long-Period (VLP) events are seismic signals which have been documented at many volcanoes throughout the world. In most cases this seismicity occurs in association with surface eruptive activity, such as at Stromboli, Italy (Neuberg et al., 1994; Chouet

* Corresponding author. Now at Istituto Nazionale di Geofisica e Vulcanologia- Sez. di Pisa. Via U. della Faggiola, 32, 56126 Pisa, Italy. Tel.: +39 050 8311960; fax: +39 050 8311942.
E-mail address: saccorotti@pi.ingv.it (G. Saccorotti).

0377-0273/$ - see front matter
doi:10.1016/j.jvolgeores.2006.10.008

Please cite this article as: Saccorotti, G. et al. Analysis of sustained long-period activity at Etna Volcano, Italy. J. Volcanol. Geotherm. Res. (2006), doi:10.1016/j.jvolgeores.2006.10.008

et al., 1997, 1999), Galeras, Colombia (Gil Cruz and Chouet, 1997), Erebus, Antarctica (Rowe et al., 1998), Soufriere Hills, Montserrat, (Neuberg et al., 1998), Usu, Japan (Matsubara and Yomogida, 2004), Popocatepetl, Mexico (Arciniega-Ceballos et al., 2000). Other observations account instead for LP-VLP signals occurring without any evident correlation with phenomena which are visible at the surface, such as at Lascar, Chile (Hellweg, 1999), Shishaldin, Alaska (Petersen et al., 2006), Tongariro, New Zealand (Hagerty and Benites, 2003), Deception, Antarctica (Ibañez et al., 2000), Kusatsu-Shirane, Japan (Kumagai et al., 2002a). Although different models have been invoked to explain the source mechanism of these events (e.g., Crosson and Bame, 1985; Chouet, 1988; Fujita et al., 1995; Jousset et al., 2003, 2004), all involve the resonance and/or transport of fluids in magmatic and hydrothermal systems. The quantitative assessment of these sources is thus critically important for our ability to model volcanic systems, and to successfully forecast eruptive activity (e.g., Chouet et al., 1994).

With a single exception (Falsaperla et al., 2002), Etna Volcano lacks significant records of long-period seismicity, mostly owing to the reduced bandwidth of the surveillance network, which was traditionally based upon 1 Hz seismometers. Volcanic signals, however, often exhibit a broadband behaviour (see references in the introduction). The undesired effects of the path and recording site are reduced when analysing Long and Very-Long-Period signals, thus permitting a direct view of the source mechanisms and mass transport phenomena. These considerations suggested the need to extend the frequency bandwidth of Etna's monitoring system, thus leading to the installation of a broadband network as a part of the permanent monitoring systems managed by the Italian National Institute for Geophysics and Volcanology (INGV hereinafter). Following this installation, sustained LP activity was observed throughout the year in 2004, accompanying a period of complete quiescence and the subsequent onset of the 'silent' 2004–2005 eruption (Burton et al., 2005).

In this paper we analyse the wavefield properties and temporal evolution of these signals, in turn retrieving precise locations for a selected subset of the most energetic events. Although our results indicate the absence of any obvious relationship between the 2004 LP swarms and the subsequent resumption of lava effusion, this study makes a significant contribution to the precise mapping of seismo-volcanic sources at Etna, thus setting the stage for the subsequent modelling efforts aimed at investigating the geometry and dynamics of the shallow plumbing system.

2. Instruments and data

Deployed by late November, 2003, INGV's broadband network at Etna consists of 8 Nanometrics TRILIUM seismometers with flat amplitude response within the 40–

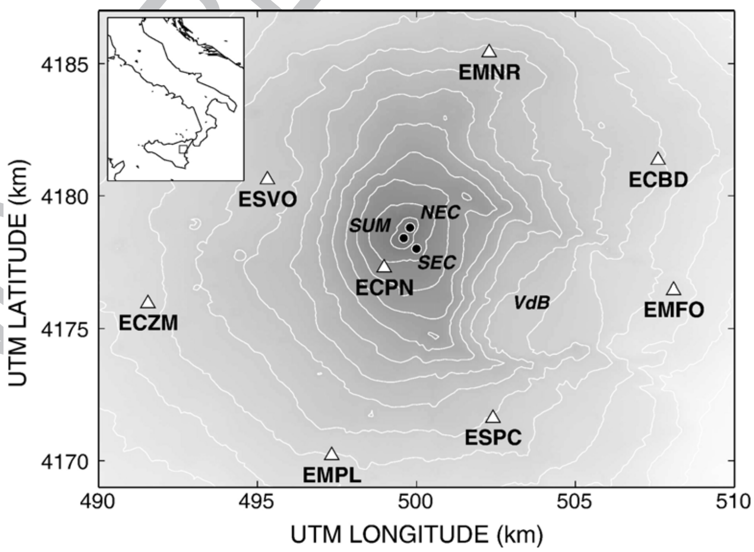

Fig. 1. Map of the summit of Etna Volcano with the location of the broadband stations of the INGV permanent monitoring network (triangles). Solid, black circles mark the position of the main craters: SUM- Summit Craters area; NEC — North-East Crater; SEC — South-East Crater. VdB indicates the Valle del Bove volcano-tectonic depression. The inset shows the location of Etna with respect to Italy.

Please cite this article as: Saccorotti, G. et al. Analysis of sustained long-period activity at Etna Volcano, Italy. J. Volcanol. Geotherm. Res. (2006), doi:10.1016/j.jvolgeores.2006.10.008

0.01 s period range, installed at elevations between 1100 and 3000 m a.s.l. and distances from the summit craters between 9 and 1.5 km (Fig. 1). Data from the remote sites are transmitted via mixed radio-satellite links to the INGV monitoring center in Catania, where they are stored with a sampling interval of 0.01 s over consecutive, 2-minute-long digital archives. These new broadband observations resulted in the detection of previously unobserved LP signals, consisting of spindle-shaped, weak pulses rapidly attenuating with distance. Most of their energy is concentrated within a narrow frequency interval spanning 0.5–10 Hz, which we attribute to a source effect based on its persistence to all the widely-spaced stations of the network (Fig. 2, top plot).

These events are superimposed on a background of continuous volcanic tremor, whose energy is concentrated within a frequency range similar to that observed for LP signals (Fig. 2, middle plot). The quantitative comparison between LP and tremor spectra must account for the filtering effects associated with both the propagation paths and the local geology beneath individual recording sites. In order to remove these unwanted contributions, we calculated network-averaged spectra for both LP and tremor signals (Fig. 2, bottom plot). Since the average station spacing is generally larger than the dominant wavelength of the signal, this procedure allows us to highlight the contributions from the primary source while removing those associated with the path and site effects. For the specific example shown in Fig. 2, LP spectra are dominated by 2 main spectral peaks at frequencies of $\approx$0.6 Hz and $\approx$3 Hz, while tremor spectra exhibit a single peak centered at a frequency of $\approx$1 Hz. This observation suggests that the continuous tremor and LP transients result from two distinct source processes.

Exploiting the different spectral signatures of LP signals with respect to those of either tremor or volcano-tectonic (VT) waveforms, we developed an automatic detection procedure based on the similarity between the spectra of triggered signals and a reference LP spectrum. Application of this procedure to data from summit station ECPN (see Fig. 1) resulted in the detection of about 56,000 LP signals spanning the November 2003–December 2004 time interval (Fig. 3a), with a peak in the maximum amplitude and daily rate between early January and late April, 2004 (Fig. 3b). The daily rate further peaked a few days before the beginning of the 2004–2005 eruption, but in association with signals much weaker than those observed during the previous months.

At the beginning of this study (early summer 2004), we had selected the data by thresholding at 155 μV the peak-to-peak amplitude of the raw vertical-component velocity seismograms from station ECPN. This first selection includes 1510 events encompassing the December 17, 2003–May 4, 2004 time span. Following the onset of the 2004–2005 eruption, we used an amplitude threshold of 75 μV for extracting additional 1430 events spanning the May 10–September 25, 2004 time interval. This second catalog, however, includes only data from summit station ECPN, as the Signal-to-Noise-Ratio (SNR) at the remaining sites was definitively too low for the application of any reliable analysis. The complete data set analysed in this paper thus amounts to 2940 events. Data were organised in digital archives containing 2-minute-long recordings starting 60 s before the maximum peak-to-peak LP amplitude measured at station ECPN. Before the analysis, data were corrected for instrument response.

3. Data analysis

3.1. Spectral properties

In order to investigate the temporal evolution of LP signals, we conducted spectral analysis over the whole catalog derived from summit station ECPN, using a 5.12 s long window encompassing the maximum peak-to-peak amplitude of the vertical-component recordings. The frequency resolution *df* of spectral estimates thus corresponds to 0.19 Hz. As mentioned above, our LP catalog was generated by an automatic classification procedure based on the spectral similarity of triggered signals with respect to a reference LP spectrum. Therefore, we expect that all the different LP spectra will exhibit a high level of mutual similarity. Following this assumption, we averaged the LP spectra on a daily basis, in turn deriving a periodogram estimate (Press et al., 1992) of the power spectrum. These power spectra were then arranged in a time-frequency representation (spectrogram) extending over the whole period spanned by our catalog (Fig. 4a). Integration over frequency of individual power spectra allowed us to obtain an estimate of the daily energy associated with the LP catalog (Fig. 4a, top plot). An average view of LP spectral signature is eventually gained by stacking the different daily power spectra (Fig. 4a, right plot).

LP spectra are dominated by a main peak at a frequency of $\approx$0.6 Hz, and higher-frequency overtones at frequencies of $\approx$2, 3.2, 5, 6.5 and 9 Hz. Although the relative weight of these peaks varies with time, most of them depict a marked persistency throughout the analysed sequence.

Starting in April, 2004, the dominant peak at $\approx$0.6 Hz broadens and appears to shift toward slightly

Please cite this article as: Saccorotti, G. et al. Analysis of sustained long-period activity at Etna Volcano, Italy. J. Volcanol. Geotherm. Res. (2006), doi:10.1016/j.jvolgeores.2006.10.008

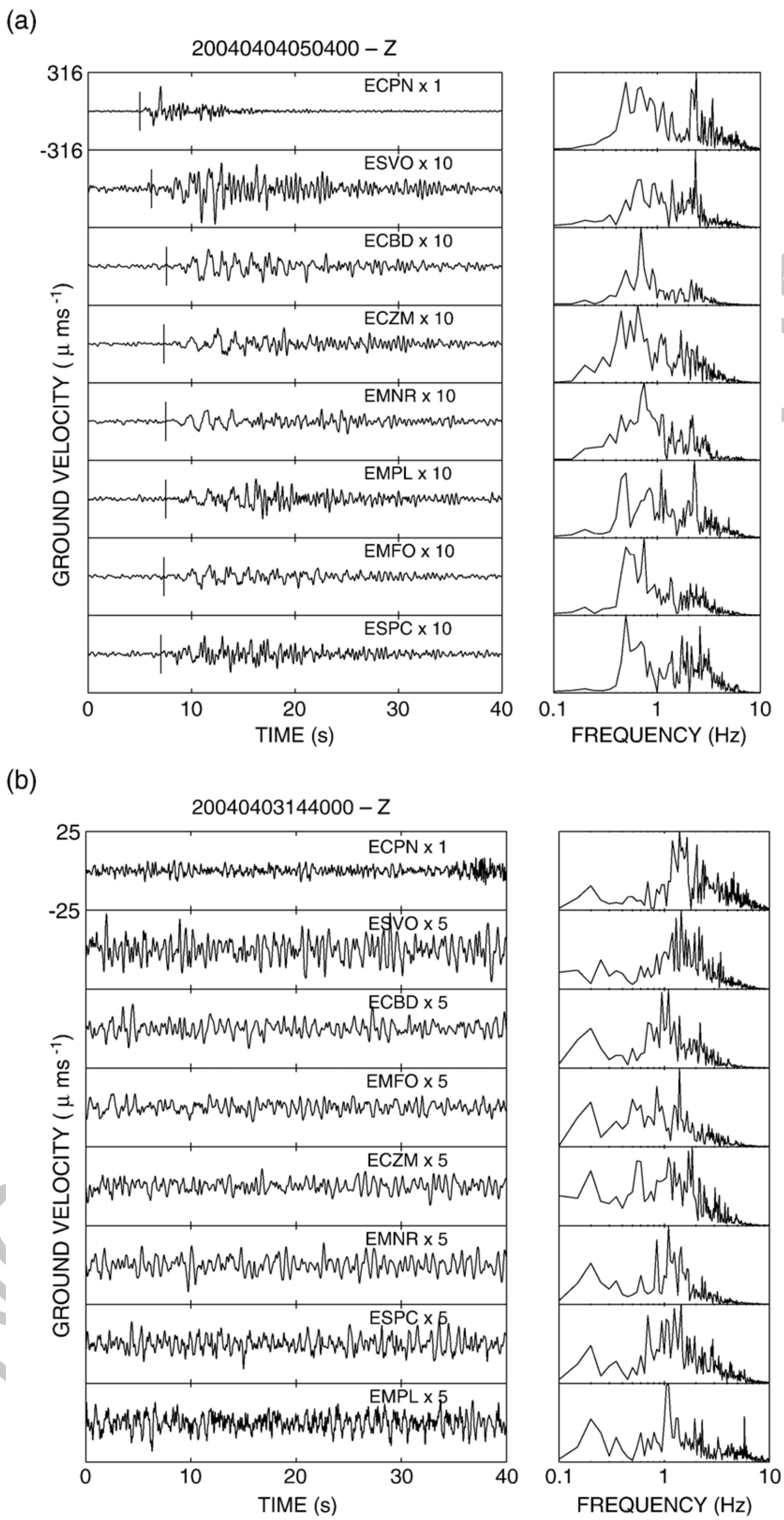

Please cite this article as: Saccorotti, G. et al. Analysis of sustained long-period activity at Etna Volcano, Italy. J. Volcanol. Geotherm. Res. (2006), doi:10.1016/j.jvolgeores.2006.10.008

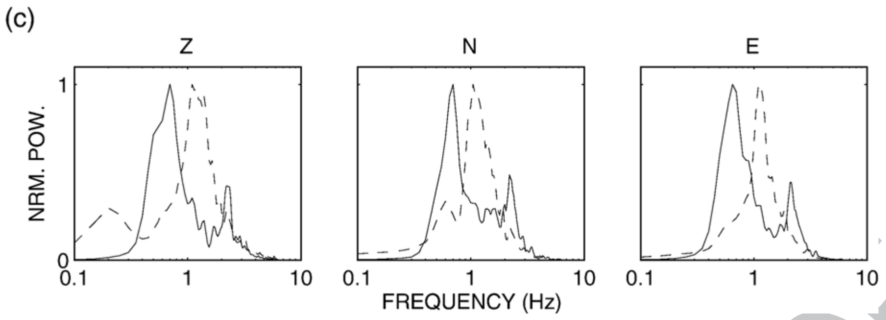

Fig. 2 (*continued*).

higher frequencies; this effect, however, is likely due to contamination of LP spectra by the tremor peak at frequency ≈ 1 Hz (see Fig. 4 2). Over the same period, in fact, LP energy decreases while the energy associated with the background gets relatively larger (Fig. 4). Moreover, it is difficult to assess such subtle frequency changes on the basis of our Fourier-based spectral measurements; the brief duration of LP signals constrains us to perform spectral estimates over short time windows, thus necessarily leading to poor frequency resolution. Any future effort aimed at investigating the fine spectral structure of our LP data should therefore be based upon techniques, such as instantaneous frequency determinations or Autoregressive Modelling of the signal (Lesage et al., 2002), which allow for the efficient separation of closely-spaced spectral peaks even over short-duration time series.

Similar analyses were conducted over tremor data, by computing spectral estimates over 5.12-s-long windows of signal taken from the beginning of the LP recordings (Fig. 4b). Tremor spectra broadens over the 1–5 Hz frequency range, and their peaks are less marked than and different from those observed for LP spectra. No noticeable variations of either the energy or spectral content of tremor signal appear to herald the onset of the 2004–2005 eruptive episode.

3.2. Waveform similarity

Although individual, raw LP signals depict quite different waveforms, once band-pass filtered around the main frequency peak they all share a common signature.

We quantified this observation by conducting correlation analyses for all the independent event pairs using 5-s-long windows encompassing the maximum peak-to-peak amplitude of the 0.1–1 Hz band-pass-filtered, vertical-component seismograms from summit station ECPN. We then scanned this large correlation matrix in ascending chronological order and extracted the elements for which the correlations among all the possible permutations were greater than the arbitrary threshold of 0.8. In this procedure, we didn't allow any overlap between clusters; in other words, once an event was assigned to a given group, it was removed from the correlation matrix thus preventing it from being associated with any other cluster. At the end of the process we then discarded the small clusters constituted by less than 5 elements, and found that 1759 out of the initial 2940 events grouped into four large families, whose temporal distributions seem to depict a weak evolutionary trend (Fig. 5a). Rather than the consecutive evolution of distinct sources, however, such a trend is probably an artifact of our sequential, exclusive clustering procedure. For each of these clusters, we used the inter-event delay times derived from correlation analyses to align seismograms, and computed stacked waveforms (e.g., Rowe et al., 2004). The stacked signals associated with the different clusters display a marked similarity (Fig. 5b), thus reinforcing the idea that individual groups are most likely representative of the same source. We also repeated the correlation and clustering procedures over the two horizontal components of ground velocity, the result of which support our findings for the vertical component case.

3.3. Polarisation analysis

Fig. 6 illustrates an example of particle motion trajectories observed at station ESVO in association

Fig. 2. Top: Vertical-component velocity seismograms for a LP event recorded by all the stations of the network, and corresponding normalised amplitude spectra calculated over a 15 s long window starting at the onset of the event (vertical lines on the seismograms). Traces are arranged in order of decreasing amplitude. Middle : Vertical-component velocity seismograms for a 40 s long section of volcanic tremor, and corresponding normalised amplitude spectra calculated over a 15 s long window. Bottom: Network-averaged normalized power spectra estimates for the three components of ground velocity associated with the LP and tremor signals shown in two panels above (continuous and dashed lines, respectively).

Please cite this article as: Saccorotti, G. et al. Analysis of sustained long-period activity at Etna Volcano, Italy. J. Volcanol. Geotherm. Res. (2006), doi:10.1016/j.jvolgeores.2006.10.008

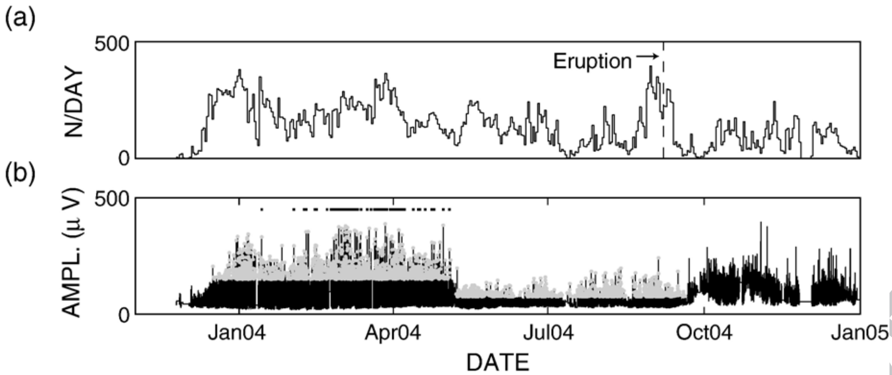

Fig. 3. Time evolution of LP activity from November 1st, 2003, through the end of 2004. (a) Daily count of events at station ECPN resulting from the automatic classification procedure. The dashed vertical line marks the onset of the 2004–2005 eruption. (b) Maximum peak-to-peak amplitude of the raw, vertical-component velocity seismograms from station ECPN. Gray dots indicate the events selected for our analysis after the application of two different amplitude thresholds. Black dots at the top of the plot mark the origin times of the events successfully located.

with the event's onset and the subsequent, largest amplitude phase. The signal initiates with a low-amplitude, quasi-horizontal rectilinear pulse; even accounting for the expected effect of topography on P-wave incidence angle, (e.g., Neuberg and Pointer, 2000), this phase is consistent with a direct P-wave arrival from a source located at shallow depths beneath the summit craters. The subsequent, largest-amplitude phase depicts instead a transverse orientation, which is compatible with a SH-Love wave arrival. The delay time between this phase

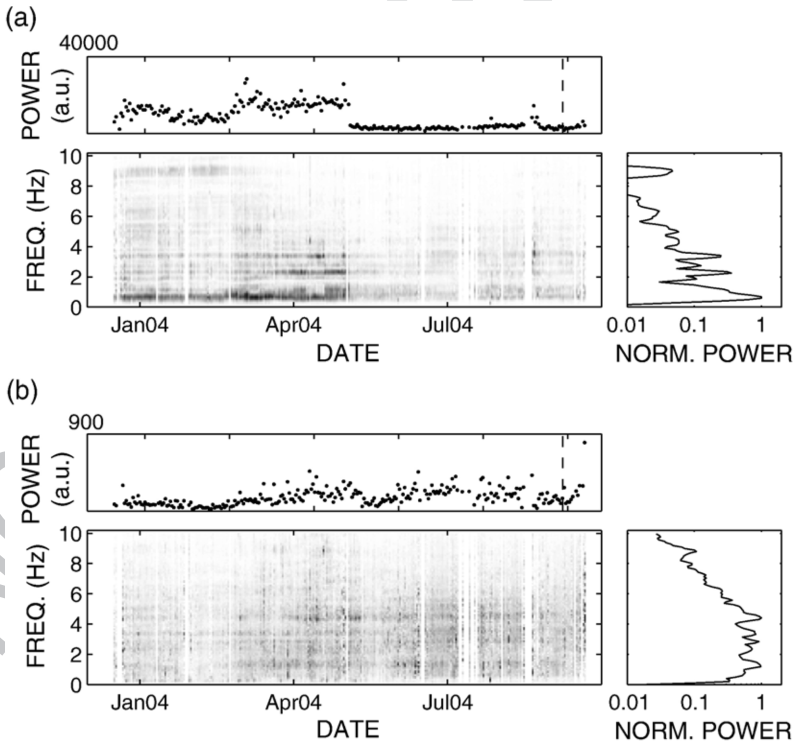

Fig. 4. (a) Spectral amplitude versus time and frequency (spectrogram) for vertical-component LP recordings at station ECPN. Each spectrogram's column represents the daily average of LP spectra calculated over 5.12 s long time windows encompassing the maximum peak-to-peak amplitude of the velocity seismograms. The top plot represents the temporal behaviour of the overall spectral power, obtained after integrating the spectrogram over frequency. The plot at the right depicts the stacked, normalised power spectrum obtained after time-integration of the spectrogram. (b) The same as in (a), but for tremor data preceding the onset of LP signals.

Please cite this article as: Saccorotti, G. et al. Analysis of sustained long-period activity at Etna Volcano, Italy. J. Volcanol. Geotherm. Res. (2006), doi:10.1016/j.jvolgeores.2006.10.008

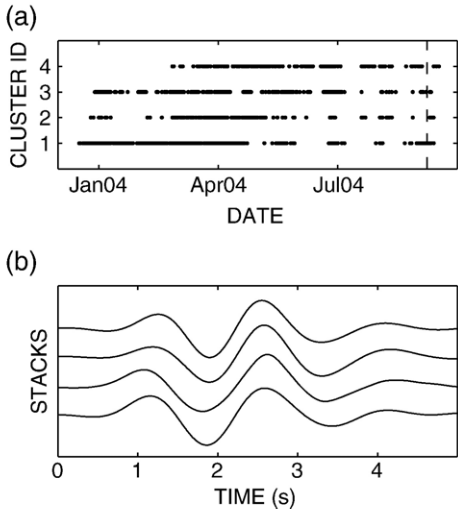

Fig. 5. (a) Temporal location of events pertaining to the four different clusters of similar events derived from correlation analysis. (b) Stacked waveforms obtained after aligning and summing vertical-component velocity seismograms pertaining to the four different clusters shown in (a).

and the P-wave onset is on the order of 5 s, thus much larger than the 1–2 s which would be expected for a direct S-wave radiated by a shallow source beneath the summit craters. For the specific example shown in Fig. 6, the origin of the large-amplitude transverse phase is thus most likely associated with a path or recording site effect. For the subset of the most energetic events used for location (see next section), we derived the polarisation attributes (azimuth and incidence angles, coefficient of rectilinearity) using the covariance-matrix method of Kanasewich (1981). Covariance estimates were obtained over 2-s-long time windows sliding with 0.1 s increments along the three-component velocity seismograms band-pass filtered over the 0.1–1 Hz frequency band. Fig. 7 illustrates the frequency distribution of particle motion azimuths associated with the onset of the signal and the subsequent largest amplitude of motion, here taken to correspond with the maximum of the largest eigenvalue of the 3-component covariance matrix. The resulting picture is quite complex: at most of the recording sites, the event's onset is dominated by radial motion, whose direction points to the summit craters. A notable exception is station ECPN (see Fig. 8), whose signals completely lack radial components. This observation may be easily interpreted when we consider that, for a source located at shallow depths beneath the summit craters, the time difference between the S- and P-wave arrivals would be much lower than the dominant period of the signal, thus hindering the possibility of P-wave discrimination on the basis of particle motion attributes. For this particular site, moreover, near-field effects are also expected to be significant. Station EMFO 22 also lacks clear radial onsets. A possible interpretation of this observation involves the combined effects of topography and structural complexities. That station is in fact located in close proximity to the NE margin of the Valle del Bove, as a consequence of which severe wave conversion and ray bending phenomena are expected (e.g., O'Brien and Bean, 2004). At several stations (e.g., ESVO, EMPL, ESPC) the polarisation azimuths associated with the largest amplitudes indicate the presence

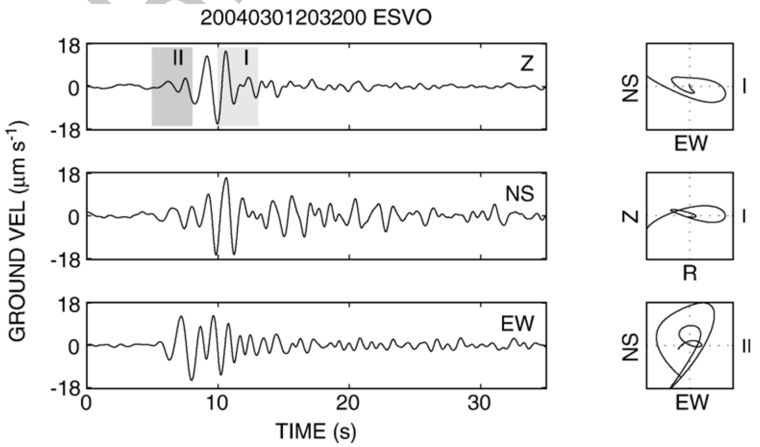

Fig. 6. Left: three-component velocity seismograms at station ESVO filtered over the 0.1–1 Hz frequency range. The two numbered gray strips mark the intervals selected for the particle motion analysis shown on the right. The onset of the LP signal (window I) is marked by a radial pulse, while the subsequent, largest-amplitude of motion (window II) is associated with shear energy.

Please cite this article as: Saccorotti, G. et al. Analysis of sustained long-period activity at Etna Volcano, Italy. J. Volcanol. Geotherm. Res. (2006), doi:10.1016/j.jvolgeores.2006.10.008

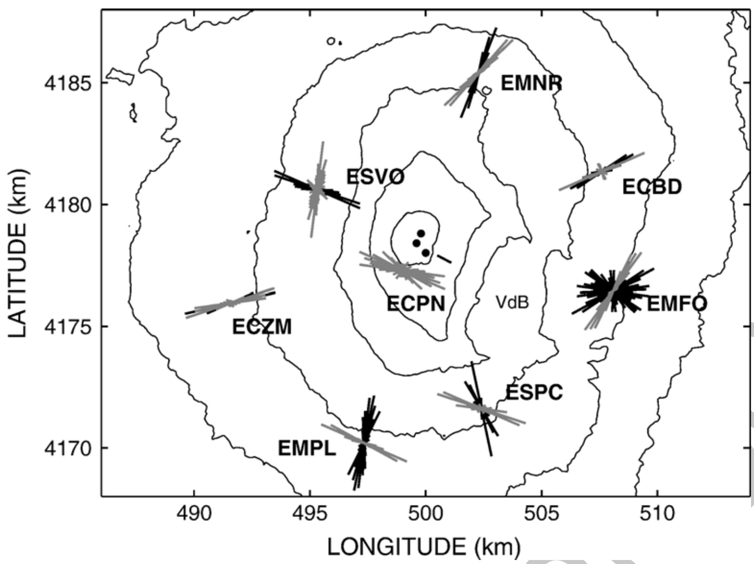

Fig. 7. Histograms of polarisation azimuths (rose diagrams) at all the stations of the network for the located events. Black and gray lines refer to the event's onset and following, largest-amplitude phases, respectively. Black dots and line mark the location of summit craters and 2004–2005 eruptive fissure, respectively.

of a large amount of shear energy. This observation may be interpreted in terms of a topography effect (e.g., Ohminato and Chouet, 1997; Ripperger et al., 2003), a source effect, or a combination of both.

At present, we are unable to evaluate the relative contributions of these two different causes in shaping the observed signal. It is worth observing, however, that the largest-amplitude polarisations depict some spatial symmetry which could be suggestive of the radiation pattern from a non-isotropic source. At sites ECZM and ECBD, which are located at opposite directions with respect to the summit craters, the largest amplitudes are associated with radial motion, while energetic shear components are observed at the ESVO-EMFO sites pair. Thus, the proximity to a P-wave nodal plane might offer an additional interpretation for explaining the lack of initial radial motion observed at station EMFO.

At present, it is impossible to speculate any further about the nature of the 12 LP source. Quantitative constraints about the geometry and dynamics of this source will hopefully be gained through future efforts aimed at retrieving the time-histories of the Moment Tensor components via full-waveform modelling (e.g., Kumagai et al., 2002b, 2005).

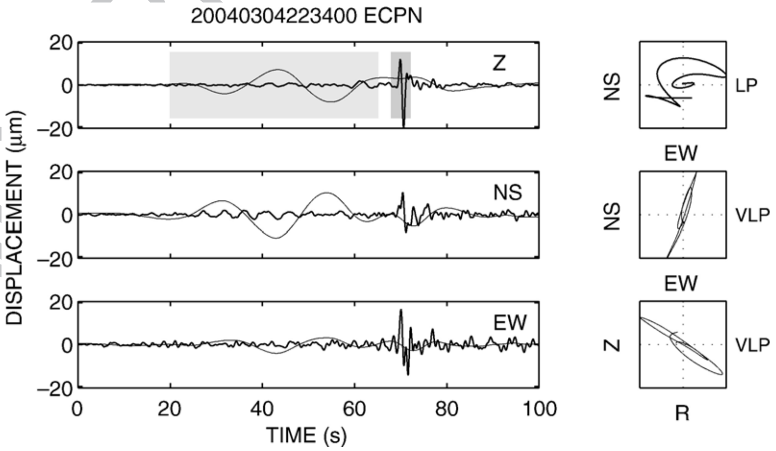

Fig. 8. Left: three-component displacement seismograms at summit station ECPN filtered over the 10–1 s (LP) and 40–10 s (VLP) period intervals (bold and thin lines, respectively). VLP data are magnified 2 times. The light and dark gray strips respectively mark the intervals selected for the VLP and LP particle motion analysis shown on the right. The onset of the LP signal is marked by a transverse pulse, while the VLP particle motion orbits point to the summit craters with a rather shallow incidence angle.

Please cite this article as: Saccorotti, G. et al. Analysis of sustained long-period activity at Etna Volcano, Italy. J. Volcanol. Geotherm. Res. (2006), doi:10.1016/j.jvolgeores.2006.10.008

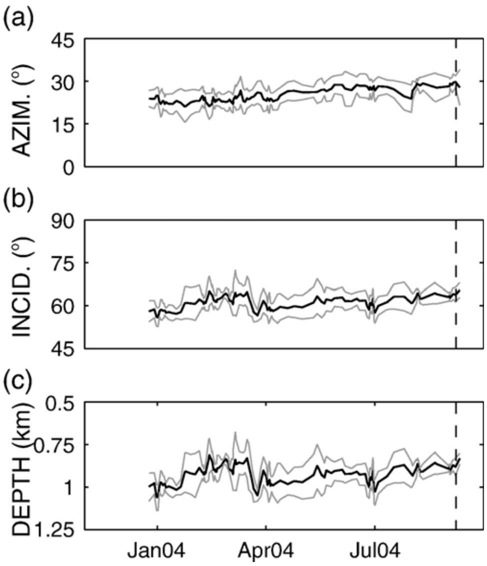

Fig. 9. Temporal evolution of azimuth (a) and incidence (b) angles for VLP pulses observed at summit station ECPN. The bold, black line is the fit to the original data, obtained by averaging subsequent groups of 40 measurements overlapping by 20. The thin, gray lines are the error bounds derived from the standard deviation of each set of observations. The plot in (c) indicates the depth of the VLP source obtained by projecting the polarisation vector onto the EW vertical plane passing through the craters. The depth is calculated with respect to the summit craters.

At station ECPN we also observed weak VLP oscillations at a period of about 20 s (Fig. 8), occurring either concurrently with or independently from the LP signals. These pulses exhibit rectilinear particle motion oriented toward the summit craters, with dominant incidence angles between 50° and 70°.

Using band-pass filtering over the 50–10 s period interval, we extended measurements of the VLP polarisation azimuth and incidence angles to all data segments from station ECPN. The low energy of these pulses means that they are not visible or cannot be analysed at the remaining recording sites.

Fig. 9 illustrates the temporal variation of the direction of VLP particle motion. By constraining the VLP sources to the EW vertical plane passing through the crater, and neglecting the particle motion distortion as a consequence of free-surface interaction (Neuberg and Pointer, 2000), we then convert VLP polarisation angles to source depths. Under such simplifying assumptions, and accounting for measurement uncertainties, the depth of the VLP source would vary between ≈750 m and ≈1100 m beneath the summit craters. The shallowest locations are associated with the January–April, 2004, interval, and with the later part of the catalog preceding the onset of the eruption. Finally, we compare the daily average of the peak-to-peak amplitudes of LP and VLP signals (Fig. 10). Within the inherent limitations due to the lack of completeness of both catalogs, significant correlation exists between the two sets of observations, thus suggesting an inter-relationship between LP and VLP seismicity.

4. Locations

Determining the location of our LP data is challenging due to the emergent onsets and poor SNR at most stations. However, the similarity of waveforms may be exploited to get consistent estimates of inter-event differential times and high-SNR stacked waveforms to be used for reliable phase-picking procedures. From the LP catalog, we used a threshold of 50 μms^{-1} on the peak-to-peak amplitude of the vertical-component velocity seismograms at station ECPN to extract the largest 123 events for which recordings by at least 6 stations were available. For these events, we used the preliminary time pickings at station ECPN to guess P-wave onsets at the remaining sites of the network, based on the travel times predicted for a source located 500 m beneath the craters. Using this set of guessed time pickings, we repeated the correlation analyses using short (2.5 s long) time windows encompassing the expected signal onset. We then applied the Equivalence Class (EC) clustering algorithm (Press et al., 1992) to the resulting correlation matrices, using a correlation threshold of 0.9. In this manner, we found that all the recordings from individual stations grouped into a single, large family. In contrast to the clustering procedure presented above, the group formed by the EC algorithm is an 'open' tree, in the sense that not every event pair in the tree needs to be correlated. Events A, B and C form a tree if (A,B) and (B,C) are correlated,

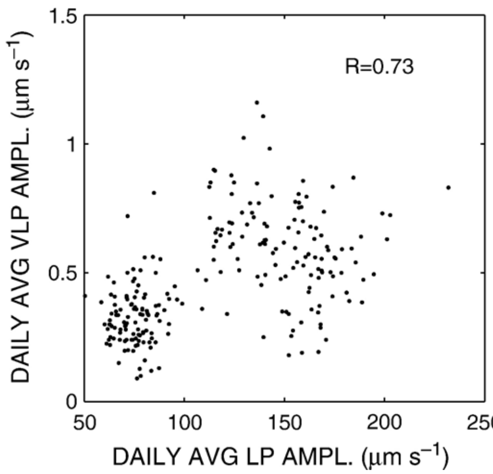

Fig. 10. Relationships between the daily-average of LP and VLP signal amplitudes.

Please cite this article as: Saccorotti, G. et al. Analysis of sustained long-period activity at Etna Volcano, Italy. J. Volcanol. Geotherm. Res. (2006), doi:10.1016/j.jvolgeores.2006.10.008

regardless the correlation between A and C. This approach is particularly advantageous for analysing large catalogues where, for a given correlation threshold, there are sets of events connected by at least one differential time path (Shearer, 1997).

For the clustered data, we used the preliminary time pickings and the precise, inter-event time delays derived from correlation analyses to derive consistent alignment of waveforms (Shearer, 1997). This procedure is expressed in matrix notation as

$$\mathbf{d} = \mathbf{G}\mathbf{m} \tag{1}$$

where the vector **d** contains the preliminary time pickings and the correlation- derived inter-event time differences; **G** is an auxiliary matrix, and **m** is a vector containing the adjusted first arrivals. For the specific case of a cluster formed by 4 events, the above equation is written explicitly as:

$$\begin{bmatrix} T_1 \\ T_2 \\ T_3 \\ T_4 \\ \Delta T_{12} \\ \Delta T_{13} \\ \Delta T_{14} \\ \Delta T_{23} \\ \Delta T_{24} \\ \Delta T_{34} \end{bmatrix} = \begin{bmatrix} 1 & 0 & 0 & 0 \\ 0 & 1 & 0 & 0 \\ 0 & 0 & 1 & 0 \\ 0 & 0 & 0 & 1 \\ 1 & -1 & 0 & 0 \\ 1 & 0 & -1 & 0 \\ 1 & 0 & 0 & -1 \\ 0 & 1 & -1 & 0 \\ 0 & 1 & 0 & -1 \\ 0 & 0 & 1 & -1 \end{bmatrix} \cdot \begin{bmatrix} t_1 \\ t_2 \\ t_3 \\ t_4 \end{bmatrix} \tag{2}$$

where T_i is the preliminary P-wave arrival for event i, and Δ_{ij} is the time difference between events i and j derived from correlation analysis. We seek a model vector **m**, containing the adjusted estimates of arrival times t, that minimizes $\mathbf{d}-\mathbf{G}\mathbf{m}$. This is solved using a weighted generalised inverse:

$$\mathbf{m} = (\mathbf{G}^T \cdot \mathbf{W} \cdot \mathbf{G})^{-1} \mathbf{G}^T \cdot \mathbf{W} \cdot d \tag{3}$$

where the matrix **W** contains weights associated with the quality of both the preliminary picks and time difference estimates. We assigned an unitary weight to all the preliminary picks, while weighting the inter-event delay times by the respective correlation coefficient c_{ij} using the relationship (Got et al., 1994):

$$W_{ij} = \frac{c_{ij}^2}{1-c_{ij}^2} \tag{4}$$

Since the number of differential time estimates is generally much larger than that of the preliminary time pickings, the arrival times derived from Eq. (3) provide a consistent alignment of waveforms, but the signal's onsets are not necessarily correct. As a last step, therefore, we derived absolute time pickings by correcting the adjusted arrival times for the visually-estimated onset of the stacked waveforms (Fig. 11; Rowe et al., 2004).

For the location procedure, we used a non-linear, probabilistic inversion (Tarantola and Vallette, 1982) acting on reciprocal travel-times calculated using finite-difference for the 3D heterogenous P-wave velocity structure of Patanè et al. (2002). In our approach, we first located the stacked event, and then used the residuals from this location as station terms for the subsequent location of the entire selected catalogue. In this manner, the systematic errors due to our incomplete knowledge of the earth structure are eliminated, while high precision in the relative positions of individual hypocenters is ensured by the previously-obtained least-square adjustment of first arrivals.

Fig. 12 displays the final locations, compared with the particle motion attributes for the VLP oscillations measured at summit station ECPN. In agreement with the similarity of waveforms, all the hypocenters are tightly clustered in a small volume extending between the surface and ≈800 m beneath the summit craters. Once accounting for the uncertainties in the hypocenter determinations, the source region of LP events thus appear to be slightly shallower than the VLP source, if one assumes the latter one to be located along the crater's axis. It is worth noting that events initially associated with the different clusters do not display any systematic location pattern. This supports the initial

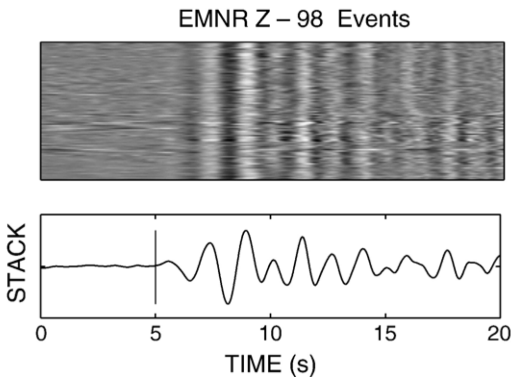

Fig. 11. Top: Vertical-component velocity seismograms for station EMNR after the least-squares adjustment procedure of arrival times. Dark and light gray tones correspond to troughs and peaks in the ground velocity time-history, respectively. Bottom: Stacked trace resulting from summation of the above seismograms. The vertical line marks the manually-picked onset. Note how the constructive summing of the aligned traces allows us to successfully recover the weak, positive first arrival, which is barely visible on the individual seismograms.

Please cite this article as: Saccorotti, G. et al. Analysis of sustained long-period activity at Etna Volcano, Italy. J. Volcanol. Geotherm. Res. (2006), doi:10.1016/j.jvolgeores.2006.10.008

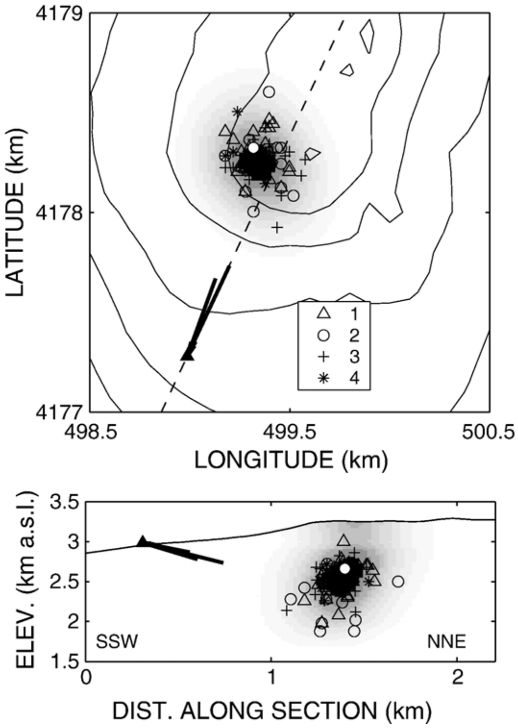

Fig. 12. Maximum-Likelihood hypocenter locations in map view (a) and projected along the vertical section passing through station ECPN (triangle) and the summit craters (b). The shaded regions bound the 90% confidence regions for hypocenter location, obtained by stacking the marginal probability distributions associated with individual events. White circles mark the location obtained from the stacked waveforms. The thick gray lines are the frequency distribution of azimuth and incidence angles for VLP pulses observed at the summit station ECPN during the time interval encompassed by the located LP events. Events pertaining to the different clusters are marked by different symbols, according to the legend shown in (a).

hypothesis that these clusters are most likely associated with slightly different excitation mechanisms of the same source, rather than being the result of spatially-distinct sources.

5. Discussion and conclusions

In this paper we described sustained LP activity occurring at Etna Volcano from November 2003 through to the end of 2004. LP amplitudes fluctuate with time, and climax during the January–April 2004 time span. The daily rate of occurrence peaked in late December, 2003, late March, 2004, and late August, 2004, a few days before the onset of the 2004–2005 eruption. This latter peak is however associated with signals of very small amplitude, and is not particularly relevant once compared to the previous ones.

Throughout the analysed time interval, LP spectra display a few, narrow peaks spanning the 0.5–10 Hz frequency band. Due to their persistence at all the widely-spaced stations of the network, we attribute the origin of these peaks to a source effect. Once band-pass filtered around the main spectral component at frequency ≈ 0.6 Hz, waveforms maintain a marked similarity throughout the analysed time interval, thus indicating the involvement of a non-destructive source process. Taken all together, these observations suggest that our LP events most likely represent the harmonic oscillation of a magmatic/hydrothermal reservoir repeatedly triggered by time-localized pressure steps (e.g., Crosson and Bame, 1985; Chouet, 1988;1996; Fujita et al., 1995; Neuberg and Pointer, 2000; Jousset et al., 2003, 2004). Within this framework, the low frequency content of

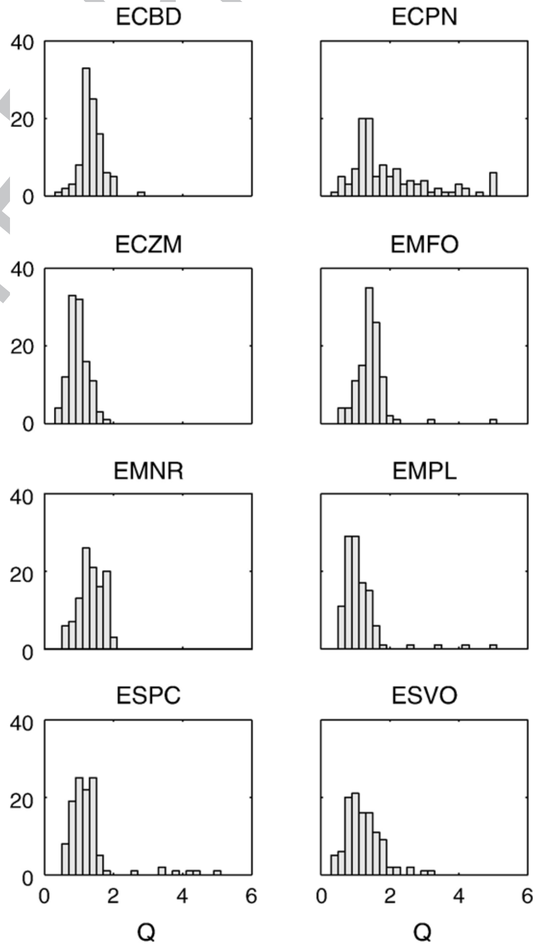

Fig. 13. Frequency distribution of Q measurements associated with the spectral peak at a frequency ≈0.6 Hz measured on the vertical components of all the stations of the network, for the set of located events.

Please cite this article as: Saccorotti, G. et al. Analysis of sustained long-period activity at Etna Volcano, Italy. J. Volcanol. Geotherm. Res. (2006), doi:10.1016/j.jvolgeores.2006.10.008

these signals would be indicative of the existence of interface waves generated at the fluid-rock boundary.

Previous studies of tremor and LP suggested that both events represented the response of the same source to different excitation mechanisms. For instance, Chouet et al. (1997) analysed tremor and LP explosion-quakes at Stromboli Volcano, Italy, and found that both signals depicted several common spectral peaks. Neuberg and Pointer (2000) analysed LP and tremor from La Soufriere Volcano, Montserrat, and observed that LP signals occur in swarms, occasionally merging in tremor episodes characterised by harmonic spectral lines shifting with time. Neuberg and Pointer (2000) modeled this observation by simulating tremor signals as the regular, repeated activation of the LP source at consecutive time intervals. Thus, at both Stromboli and La Soufriere volcanoes, LPs and tremor appear to share the same source process, and would represent the response of the same resonator to transient or repeated excitation mechanisms, respectively.

In contrast, the spectral analyses presented for our Etna data do not depict any common peak between LP and tremor spectra. Moreover, detailed time-frequency analyses (not shown here) indicate that the tremor-LP transition is marked by an abrupt change of the spectral signature, without any evidence of shifting spectral lines. These observations thus suggest that, during the period of our observations, LPs and tremor at Etna originated from two distinct source processes and/or locations. Corroborating this hypothesis are the results from a recent study by Di Grazia et al. (2006), who retrieved tremor locations at Etna throughout the year 2004. For the period relevant to the present work (early April, 2004) the tremor sources imaged by Di Grazia et al. (2006) are clustered beneath the summit craters, at elevations around 1600 m (see their Fig. 2), and thus considerably deeper than the source centroid of our LP signals. These observations thus point to a complex plumbing system, where different portions of the summit conduits' network are affected by different dynamical processes, thus generating distinct classes of signals.

The quantitative investigation about the geometry and dynamics of the LP source requires a definition of the time-history of the Moment-Tensor and Single-Force components via full-waveform modelling of the signals (e.g., Kumagai et al., 2002b; Nakano et al., 2003; Kumagai et al., 2005). Some of the observations presented above, however, already give hints about the geometry of the LP source. LP models have been proposed accounting for spherical (e.g., Crosson and Bame, 1985; Fujita et al., 1995) or cylindrical (Chouet, 1985) geometries. The large amount of shear energy, and the non-isotropic radiation pattern observed during our polarisation analysis can be explained, however, only by invoking a crack-like geometry (Chouet, 1988), as it is the only source geometry which is able to generate a significant amount of shear waves. Chouet (1988) showed that the fluid-filled crack generates a very slow wave, that he called the crack wave, which leads to more realistic estimates of the size of the resonator than those associated with the spherical geometry. Moreover, the crack-like geometry is also appropriate for mass transport conditions beneath a volcano. Under this perspective, the unevenly-spaced peaks observed in our LP spectra would be representative of the different longitudinal and transverse modes of vibration of the crack.

Following the resonating-fracture hypothesis, hints about the composition and physical properties of the fluid contained in the crack may be gained through examination of the quality factor Q of the resonator, that we measure from LP spectral estimates using the relationship:

$$Q = \frac{f}{\Delta f} \tag{5}$$

where f is the frequency corresponding to a given spectral peak and Δf is the width of that peak at half the peak's magnitude. We applied Eq. (5) to the dominant peak at a frequency ≈ 0.6 Hz separately to the three components of motion for the set of located events, obtaining similar results. Therefore, in Fig. 13 we only show results for the vertical component. All the stations of the network yield consistent results, with distributions of Q peaked at values around. This value is significantly smaller than those observed at other volcanoes. Q estimates from the literature span in fact the 10–500 range, the lower and upper bounds being associated with LPs observed at Kilauea volcano, Hawaii (Kumagai et al., 2005) and Galeras volcano, Colombia (Kumagai and Chouet, 1999). The quality factor is made up by two terms: $Q^{-1} = Q_i^{-1} + Q_r^{-1}$, where Q_i^{-1} expresses the intrinsic attenuation in the fluid, and Q_r^{-1} refers to energy losses at the fluid-rock interface.

Using Chouet's (1988) crack model, Kumagai and Chouet (1999, 2000) performed a detailed investigation of the acoustic properties of a fluid-filled fracture under a variety of fluid and rock-matrix properties, in turn examining (Kumagai and Chouet, 2001) the dependence of such properties on the crack geometry and vibration modes. These studies demonstrated that the wide range spanned by Q measurements may be explained in terms of the different physical properties of the multiphase

Please cite this article as: Saccorotti, G. et al. Analysis of sustained long-period activity at Etna Volcano, Italy. J. Volcanol. Geotherm. Res. (2006), doi:10.1016/j.jvolgeores.2006.10.008

fluid mixtures and the surrounding rock matrix. Although Kumagai and Chouet's results demonstrated that the association between a given Q value and the composition and physical properties of the fluid may be manifold, their conclusions indicate that the high decay rate observed for our LP events can only be explained in terms of a low impedence contrast at the fluid-rock interface which prevents the trapping of elastic energy inside the fissure.

Several multiphase mixtures may fulfill such a condition; however, the absence of any surface-visible phenomena indicates that the most likely candidate for the LP source is a crack filled with a basalt-gas or water-vapour mixtures at very low gas-volume fractions. For instance, a bubbly basalt at gas-volume fraction close to 0 and pressures between 5 and 20 MPa (thus encompassing the 13–17 MPa range which is expected at LP's hypocentral depths) yields Q_r^{-1} over the 0.1–1 range (see Fig. 13 in Kumagai and Chouet, 2000), and Q_i^{-1} between 0.06 and 0.001. For this particular fluid, therefore, the total Qwould be in the 1–10 range. Similarly, a fracture filled by bubbly water at 1–1.5% gas-volume fraction would depict Q_r^{-1} and Q_i^{-1} spanning the 0.2–1 and 0.05–0.001 ranges, respectively, thus resulting in a Q between 1 and 5.

The temporal trends of the acoustical properties (attenuation and dominant frequency) have important implications for monitoring the volcano. Temporal changes of such parameters may in fact be interpreted in terms of variations in the physical properties of the multiphase mixtures filling the resonating cavity (e.g., Kumagai et al., 2002a; Jousset et al., 2003; De Angelis and McNutt, 2005). Within the measurement limitations inherent the low amplitude and short duration of the signals, the spectral signatures of our LP data appear to be invariant with time (Fig. 4). Moreover, the marked similarity of waveforms throughout the analysed time interval suggests that the attenuation at the source remained roughly constant as well. Taken all together, these observations indicate that the physical conditions of the upper conduit system feeding the summit craters didn't suffer any remarkable variation during the months preceeding the eruption, in turn pointing to a general lack of correlation between the LP-generating process and the renewal of effusive activity. These arguments thus support the hypothesis that both the feeding system and triggering mechanism of the 2004– 2005 eruption were poorly related to the dynamics of the main plumbing system feeding the summit craters. Rather, the lack of any significant seismological precursor (Di Grazia et al., 2006) and the petrological/geochemical properties of the extruded lavas (Burton et al., 2005) suggest that this eruption was mostly controlled by geodynamic stresses acting on a lateral reservoir filled by degassed, resident magma. Additional work is required to put further constraints on these hypotheses: future studies will therefore concern detailed analysis of the dominant frequencies and decaying rate of LP waveforms, using methods with greater resolving power than the Fourier-based spectral estimates adopted in this work. Of particular promise is the *Sompi* method which, based on an auto-regressive 24 equation, addresses the problem of resolving the decaying harmonic components of a time series corrupted by noise (Kumazawa et al., 1990; Nakano et al., 1998). Moreover, the correct interpretation of the acoustic properties in terms of fluid characteristics requires the assessment of the LP source geometry and dynamics. This latter task may be approached using moment-tensor inversion from full-waveform modelling of the most energetic signals. A major challenge in this respect is the calculation of Green's function which, as suggested by our polarisation analysis, must necessarily account for the effects of topography on wave propagation.

During our analyses, we also found a significant correlation between the amplitudes of LP and VLP signals. Taken together with the proximity of the respective source regions, these observations suggest that a close link must exist between the two phenomena. Recent studies (e.g., Chouet, 2003, and references therein) indicate that VLP signals most likely represent the dynamic response of the host rock to mass transport processes in volcanic conduits, such as the sudden decompression of large gas bubbles as they approach the terminal part of a magmatic column.

Quantitative estimates about the volumetric changes associated with this kind of process would require determination of the Moment-Tensor components, a task which is made impossible by the extremely poor SNR exhibited by these events at all the peripheral stations of the network. With the data presently available, a rough estimate of the volume changes at the VLP source can only be attempted by fixing the source location and assuming a source of geometry. Under these simplifying conditions, we considered an explosive (isotropic) point source located at the barycenter of the LP sources, i.e. at a distance and depth of 1000 m and 500 m, respectively, from summit station ECPN. Using the classic Stokes' solution (Aki and Richards, 2002), we then calculated the Green's functions for an isotropic point source, using V_p=3000 m s^{-1}, V_p/V_s ratio of $\sqrt{3}$, and rock density of 2500 kg m^{-3}. In this manner, we found that the typical radial displacement of ≈10 μm observed at station ECPN would correspond to an isotropic moment M_i on

Please cite this article as: Saccorotti, G. et al. Analysis of sustained long-period activity at Etna Volcano, Italy. J. Volcanol. Geotherm. Res. (2006), doi:10.1016/j.jvolgeores.2006.10.008

the order of $\approx 4\times10^{12}$ Nm. The isotropic moment is related to the volume change ΔV at the source by the relationship (Aki and Richards, 2002):

$$M_i = \Delta V(\lambda + 2\mu) \tag{6}$$

where λ and μ are Lame's elastic coefficients. Assuming $\lambda = 2\,\mu$, and $\mu = 7.5$ GPa, from the above relationship we obtain a ΔV on the order of 1.5×10^2 m^3. This value is smaller than, but comparable to, the ≈ 200 m^3 volumetric changes associated with Strombolian explosions at Stromboli volcano (Chouet, 2003). Our estimates thus reinforce the hypothesis that the weak VLP events observed at Etna could actually be representative of a mass-transport process involving the movement and associated decompression of gas slugs as they approach the terminal part of the magmatic column. Under this perspective, the injection of these fluids into an overlying cavity filled by either magmatic or hydrothermal fluids at poor gas volume fraction would drive the periodic pressurisation steps of such a shallow reservoir, thus triggering its resonant, LP oscillations.

In a previous work, Falsaperla et al. (2002) performed a detailed study of LP swarms occurred during the 1991–1993 eruption of Mt. Etna. These swarms were temporally correlated with episodic collapses of the NE crater floor, and originated in a region located slightly east of the NE crater, extending from the surface to a depth of 2000 m. These events depicted narrow spectral peaks spanning the 1–5 Hz frequency range, and fairly low quality factors ($Q = 13–18$). Falsaperla et al. (2002) used these features to develop a fluid-filled crack model of the source, in turn postulating that the locus of LP events was most likely associated with a dyke connecting the NE crater to a depressurizing magma body. Falsaperla et al. (2002) postulated that the repeated collapse of the overlaying crater floor could have induced the transient pressurisations of that dyke, thus triggering its resonant, LP oscillations.

These past results, and the ones presented in this work, provide two interesting case studies demonstrating the variety of dynamical processes acting as source of LP seismic waves. The quantitative assessment of these processes thus represent a fundamental step toward a better understanding of volcanic systems, in turn constituting a critical improvement in our ability to successfully forecast eruptive activity.

Acknowledgments

The paper benefited from many thoughtful comments by P. Jousset and 4 anonymous reviewers. Luciano Zuccarello is greatly acknowledged for his constant helping hand during the data retrieval procedure. This work was financed 6 by the INGV-Department for Civil Protection and EU 6th framework project 7 *VOLUME*. Ivan Lokmer is supported by the EU 6th framework Marie Curie 8 RTN, *SPICE*.

References

Aki, K., Richards, P.G., 2002. Quantitative Seismology, second ed. University Science Books, Sausalito (CA). 700 pp.

Arciniega-Ceballos, A., Valdes-Gonzalez, C., Dawson, P., 2000. Temporal and spectral characteristics of seismicity observed at Popocatepetl volcano, central Mexico. J. Volcanol. Geotherm. Res. 102, 207–216.

Burton, M.R., Neri, M., Andronico, D., Branca, S., Caltabiano, T., Calvari, S., Corsaro, R.A., Del Carlo, P., Lanzafame, G., Lodato, L., Miraglia, L., Salerno, G., Spampinato, L., 2005. Etna 2004–2005: an archetype for geodynamically-controlled effusive eruptions. Geophys. Res. Lett. 32 (L09303). doi:10.1029/2005GL022527.

Chouet, B.A., 1985. Excitation of a buried magmatic pipe: a seismic source model for volcanic tremor. J. Geophys. Res. 90, 1881–1893.

Chouet, B.A., 1988. Resonance of a fluid-driven crack: radiation properties and implications for the source of long-period events and harmonic tremor. J. Geophys. Res. 93, 4375–4400.

Chouet, B.A., 1996. Long-Period volcano seismicity: its source and use in eruption forecasting. Nature 380, 309–316.

Chouet, B.A., 2003. Volcano Seismology. PAGEOPH 160, 739–788.

Chouet, B.A., Page, R.A., Stephens, C.D., Lahr, J.C., Power, J.A., 1994. Precursory swarms of long-period events at Redoubt Volcano (1989–1990), Alaska: their origin and use as a forecasting tool. J. Volcanol. Geotherm. Res. 62, 95–135.

Chouet, B.A., Saccorotti, G., Martini, M., Dawson, P.B., De Luca, G., Milana, G., Scarpa, R., 1997. Source and path effects in the wavefields of tremor and explosions at Stromboli volcano, Italy. J. Geophys. Res. 102, 15129–15150.

Chouet, B.A., Saccorotti, G., Dawson, P., Martini, M., Scarpa, R., De Luca, G., Milana, M., Cattaneo, M., 1999. Broadband measurements of the sources of explosions at Stromboli Volcano, Italy. Geophys. Res. Lett. 26 (13), 1937–1940. doi:10.1029/1999GL900400.

Crosson, R.S., Bame, D.A., 1985. A spherical source model for low-frequency volcanic earthquakes. J. Geophys. Res. 90, 10237–10247.

De Angelis, S., McNutt, S.R., 2005. Degassing and hydrothermal activity at Mt. Spurr, Alaska during the summer of 2004 inferred from the complex frequencies of long-period events. Geophys. Res. Lett. 32 (L12312). doi:10.1029/2005GL022618.

Di Grazia, G., Falsaperla, S., Langer, H., 2006. Volcanic tremor location during the 2004 Mt. Etna lava effusion. Geophys. Res. Lett. 33 (L04304). doi:10.1029/2005GL025177. Di Grazia, G., Falsaperla, S., Langer, H., 2006. Volcanic tremor location during the 2004 Mount Etna lava effusion. Geophys. Res. Lett. 33.

Falsaperla, S., Privitera, E., Chouet, B.A., Dawson, P.B., 2002. Analysis of long-period events recorded at Mt. Etna (Italy) in 1992, and their relationship to eruptive activity. J. Volcanol. Geotherm. Res. 114, 419–440.

Fujita, E., Ida, Y., Oikawa, J., 1995. Eigen oscillation of a fluid sphere and source mechanism of harmonic volcanic tremor. J. Volcanol. Geotherm. Res. 69, 365–378.

Gil Cruz, F., Chouet, B.A., 1997. Long-Period events: the most characteristic seismicity accompanying the emplacement and extrusion of a lava dome in Galeras Volcano, Colombia, in 1991. J. Volcanol. Geotherm. Res. 77, 121–158.

Got, J.L., Frechet, J., Klein, F.W., 1994. Deep fault geometry inferred from multiplet relative relocation beneath the South flank of Kilauea. J. Geophys. Res. 99, 15375–15386.

Hagerty, M., Benites, R., 2003. Tornillos beneath Tongariro Volcano, New Zealand. J. Volcanol. Geotherm. Res. 125, 151–169.

Hellweg, M., 1999. Seismic signals from Lascar Volcano. J. South Am. Earth Sci. 12, 123–133.

Ibañez, J.M., Del Pezzo, E., Almendros, J., La Rocca, M., Alguacil, G., Ortiz, R., García, A., 2000. Seismovolcanic signals at Deception Island volcano, Antarctica: wave field analysis and source modeling. J. Geophys. Res. 105, 13905–13932.

Jousset, P., Neuberg, J., Sturton, S., 2003. Modelling the time-dependent frequency content of low-frequency volcanic earthquakes. J. Volcanol. Geotherm. Res. 128, 201–223.

Jousset, P., Neuberg, J., Jolly, A., 2004. Modelling low-frequency volcanic earthquakes. In a visco-elastic medium with topography. Geophys. J. Int. 159, 776–802.

Kanasewich, E.R., 1981. Time sequence Analysis in Geophysics. University of Alberta Press, Edmonton, pp. 1–532.

Kumagai, H., Chouet, B.A., 1999. The complex frequencies of long-period seismic events as probes of fluid composition beneath volcanoes. Geophys. J. Int. 138, F7–F12.

Kumagai, H., Chouet, B.A., 2000. Acoustic properties of a crack containing magnetic or hydrothermal fluids. J. Geophys. Res. 105, 25493–25512.

Kumagai, H., Chouet, B.A., 2001. The dependence of acoustic properties of a crack on the resonance mode and geometry. Geophys. Res. Lett. 28, 3325–3328.

Kumagai, H., Chouet, B.A., Nakano, M., 2002a. Temporal evolution of a hydrothermal system in Kusasutsu-Shirane Volcano, Japan, inferred from the complex frequencies of long-period events. J. Geophys. Res. 107 (2236). doi:10.1029/2001JB000653.

Kumagai, H., Chouet, B.A., Nakano, M., 2002b. Waveform inversion of oscillatory signatures in long-period events beneath volcanoes. J. Geophys. Res. 107 (2301). doi:10.1029/2001JB001704.

Kumagai, H., Chouet, B.A., Dawson, P.B., 2005. Source process of a long period event at Kilauea volcano, Hawaii. Geophys. J. Int. 161, 243–254.

Kumazawa, M., Ymanishi, Y., Fukao, Y., Furumoto, M., Yamamoto, Y., 1990. A theory of spectral analysis based on the characteristic property of a linear dynamic system. Geophys. J. Int. 101, 613–630.

Lesage, P., Glangeaud, F., Mars, J., 2002. Applications of autoregressive models and time-frequency analysis to the study of volcanic tremor and long period events. J. Volcanol. Geotherm. Res. 114, 391–417.

Matsubara, W., Yomogida, M., 2004. Source process of low-frequency earthquakes associated with the 2000 eruption of Mt. Usu. J. Volcanol. Geotherm. Res. 134, 223–240.

Nakano, M., Kumagai, H., Kumazawa, M., Yamaoka, K., Chouet, B.A., 1998. The excitation and characteristic frequency of the long-period volcanic event: an approach based on an inhomogeneous autoregressive model of a linear dynamic system. J. Geophys. Res. 103, 10031–10046.

Nakano, M., Kumagai, H., Chouet, B.A., 2003. Source mechanism of long period events at Kusatsu-Shirane Volcano, Japan, inferred from waveform in version of effective excitation functions. J. Volcanol. Geotherm. Res. 122, 149–164.

Neuberg, J., Pointer, T., 2000. Effects of volcano topography on seismic broadband waveforms. Geophys. J. Int. 143, 239–248.

Neuberg, J., Luckett, R., Ripepe, M., Braun, T., 1994. Highlights from a seismic broadband array on Stromboli Volcano. Geophys. Res. Lett. 21, 749–752.

Neuberg, J., Baptie, B., Luckett, R., Stewart, R., 1998. Results from the broad-band seismic network on Montserrat. Geophys. Res. Lett. 25, 3661–3664.

O'Brien, G.S., Bean, C.J., 2004. A 3D discrete numerical elastic lattice method for seismic wave propagation in heterogeneous media with topography. Geophys. Res. Lett. 31 (L14608). doi:10.1029/2004GL020069.

Ohminato, T., Chouet, B.A., 1997. A free-surface boundary condition for including 3D topography in the finite-difference method. Bull. Seismol. Soc. Am. 87, 494–515.

Patanè, D., Chiarabba, C., Cocina, O., De Gori, P., Moretti, M., Boschi, E., 2002. Tomographic images and 3D earthquake locations of the seismic swarm preceding the 2001 Mt. Etna eruption: evidence for a dyke intrusion. Geophys. Res. Lett. 29 (10). doi:10.1029/2001GL014391.

Petersen, T., Caplan-Auerbach, J., McNutt, S.R., 2006. Sustained long period seismicity at Shishaldin Volcano, Alaska. J. Volcanol. Geotherm. Res. 151, 365–381.

Press, W., Teukolsky, S.A., Vetterling, W.T., Flannery, B.P., 1992. Numerical Recipes. Cambridge Academic Press.

Ripperger, J., Igel, H., Wassermann, J., 2003. Seismic wave simulation in the presence of real volcano topography. J. Volcanol. Geoterm. Res. 128, 31–44.

Rowe, C.A., Aster, R.C., Kyle, P.R., Schlue, J.W., Dibble, R.R., 1998. Broadband recording of Strombolian explosions and associated very-long-period seismic signals on Mount Erebus Volcano, Ross Island, Antarctica. Geophys. Res. Lett. 25, 2297–2300.

Rowe, C.A., Thurber, C.H., White, R.A., 2004. Dome growth behavior at Soufriere Hills Volcano, Montserrat, revealed by relocation of volcanic event swarms, 1995–1996. J. Volcanol. Geotherm. Res. 134, 199–221.

Shearer, P.M., 1997. Improving local earthquake locations using the L1-norm and waveform cross-correlation: application to the Whittier Narrows, California, aftershock sequence. J. Geophys. Res. 102, 8269–8283.

Tarantola, A., Vallette, B., 1982. Inverse problem = quest for information. J. Geophys. 50, 159–170.

Please cite this article as: Saccorotti, G. et al. Analysis of sustained long-period activity at Etna Volcano, Italy. J. Volcanol. Geotherm. Res. (2006), doi:10.1016/j.jvolgeores.2006.10.008